eprints@whiterose.ac.uk
https://eprints.whiterose.ac.uk/

Failure investigation of hybrid double-lap shear bolted connections with additively manufactured 316L stainless steel inner plates

Hasan Almuhanna [a], Giacomo Torelli [a], Renan Kindermann [b], Luca Susmel [c],*

[a] School of Mechanical, Aerospace and Civil Engineering, The University of Sheffield, Mapping Street, Sheffield S1 3JD, UK
[b] Henry Royce Institute, The University of Manchester, Oxford Road, Manchester M13 9PL, UK
[c] Materials and Engineering Research Institute, Sheffield Hallam University, Harmer Building, Sheffield S1 1WB, UK

ABSTRACT

The growing body of research on additive-manufactured components in structural engineering highlights the importance of assessing their potential, particularly in understanding how key manufacturing and design parameters influence performance. In this context, alongside conventional inner plates, this study investigates the failure behaviour of additive-manufactured inner plates of 316L stainless steel as hybrid component in double-lap shear bolted configurations. Two distinct printing methods were considered: wire arc additive manufacturing and selective laser melting. The study considered different surface conditions (as-built and machined) and extraction/print direction ($\theta = 0°$, $45°$, $60°$ and $90°$). By evaluating the actual failure mode and cracking behaviour, this study explores the influence of the manufacturing process and variations in geometrical design parameters, treated as key variables affecting the failure mechanism of the inner plates. The findings indicate that while the test coupons exhibited significant variations in stiffness and ductility, the failure behaviour of conventional and additively manufactured inner plates remained largely similar when accounting for surface condition and printing direction. Differences in load capacity across manufacturing methods were found to be limited when thickness was controlled. However, distinctly different crack propagation paths were observed in as-built wire arc additive-manufactured inner plates extracted at $\theta = 45°$ and $60°$, attributed to the effect of diagonal printing layers. These insights contribute to understanding overall connection integrity and highlight both the challenges and opportunities of integrating additive manufacturing into bolted connections.

1. Introduction

Additive manufacturing (AM) is increasingly being adopted in the construction industry as an alternative to traditionally produced materials, offering advantages in design optimisation and performance [1] and [2]. The integration of AM into construction practices aligns with advancements in industries such as aerospace and automotive manufacturing, ensuring that construction does not lag in innovation and productivity. AM offers several key potential benefits to the construction industry, including enhanced production efficiency, reduced material waste, improved precision in both off-site and on-site fabrication, and its utilisation as a solution for

Nomenclature

AM
Additive manufacturing
CON
Conventionally made
WAAM
Wire and arc additive manufacturing
SLM
Selective laser melting
DED
Direct energy deposition
PBF
Powder bed fusion
MIG
Metal Inert gas
θ
Extraction/Print direction
EB
Edge bearing
NST
Net-section tension
SO
Shear-out
BT
Block tearing
σ
Stress
$\sigma_{0.2}$
Offset yield stress
σ_u
Ultimate stress
R_a
Average surface roughness
t
Plate thickness
l
Length of the plate
b
Breadth of the plate
p
Pitch distance
e_1
End distance
e_2
Edge distance
d_o
Hole diameter
E
Modulus of elasticity
ε
Strain
ε_u
Strain at maximum stress
ε_f
Fracture strain
n
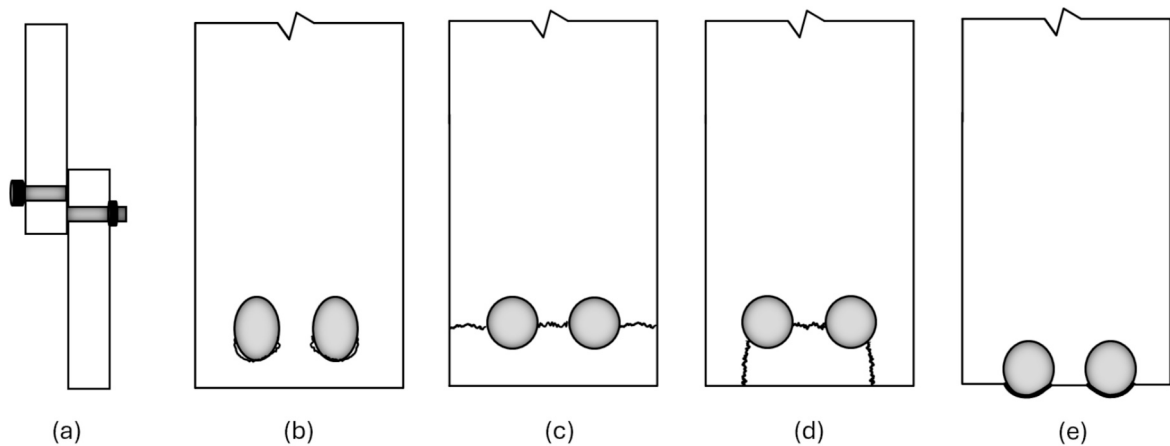Strain hardening exponent
K
Strength coefficient

Fig. 1. Failure modes of plates in bolted connections: (a) BS, (b) EB, (c) NST, (d) BT, and (e) SO.

Table 1
Typical chemical composition of 316L stainless steel raw material obtained from different production methods.

Material condition	Chemical composition, (wt%)						
	C	Si	Mn	Cr	Ni	Mo	N
Wrought	0.02	0.45	0.91	17.20	10.00	2.04	0.05
Wire	0.015	0.45	1.60	18.50	12.00	2.60	0.04
Powder	0.02	0.71	0.75	17.87	12.70	2.36	0.10

Table 2
Mechanical properties of 316L stainless steel raw material obtained from different production methods according to supplier datasheets.

Material condition	Offset yield stress, $\sigma_{0.2}$ (MPa)	Ultimate stress, σ_u (MPa)	Elongation (%)
Wrought	340	656	53
Wire	430	580	38
Powder	540	615	39

repairing structural defects [3]. Furthermore, AM materials have the potential to expand design possibilities for hybrid applications and various structural configurations. However, challenges remain in the adoption AM components, including the limited availability of standards and guidelines to guide engineering design.

In response to increasing demand, the BS EN ISO/ASTM 52,900 standard was published to define general terms, seven processing categories, and processing data relevant to additive manufacturing [4]. The standard classifies wire arc additive manufacturing (WAAM) under the direct energy deposition (DED) category, which involves material fusion through melting during deposition. A limitation of this standard is that it does not specifically address selective laser melting (SLM) but instead covers the broader powder bed fusion (PBF) category, under which SLM is classified as a sub-method. Additionally, ASTM F3187-16, last updated in February 2024, serves as a guideline for DED sub-methods [5]. It defines deposition methods for DED sub-methods, which utilise either Metal Inert Gas (MIG) welding or an electron beam. In the case of WAAM, deposition is typically carried out using an inert gas arc system.

Recent studies [6–14] have primarily focused on the two prominent AM approaches: WAAM and SLM. Metals produced using these techniques have been extensively tested and evaluated for use in structural buildings and other applications. These studies have examined print parameters, mechanical behaviour, and microstructural characteristics.

In terms of printing capabilities, WAAM is the most suitable AM technique for producing structural components, as it enables the fabrication of large-scale structural elements and allows for the production of standard steel structural geometries [15]. Additionally, unlike PBF sub-methods such as electron-beam melting (EBM) and selective laser melting (SLM), WAAM does not require a vacuum or an inert gas atmosphere. A study conducted by Ron et al. [16], highlighted notable disadvantages of using EBM and SLM, including the high cost of raw powder materials and significant energy consumption compared to WAAM. Moreover, WAAM provides substantially higher deposition rate, ranging from 4 to 9 kg/h, whereas PBF methods typically achieve only 50 g/h [3]. Nevertheless, PBF sub-methods like SLM offers superior dimensional accuracy and improved surface finish compared to other AM methods including WAAM making SLM more suitable for complex geometries requiring precise fabrication [17]. However, the performance of SLM-produced metals in structural components such as bolted connections remains largely unexplored. Therefore, examining their performance in hybrid joints and comparing their mechanical behaviour with conventional (CON) and WAAM counterparts is necessary for a comprehensive assessment of their potential.
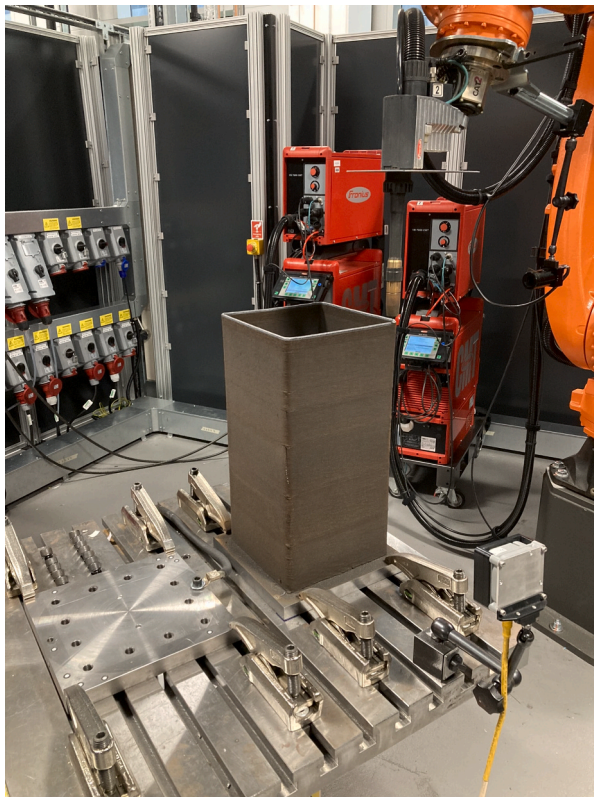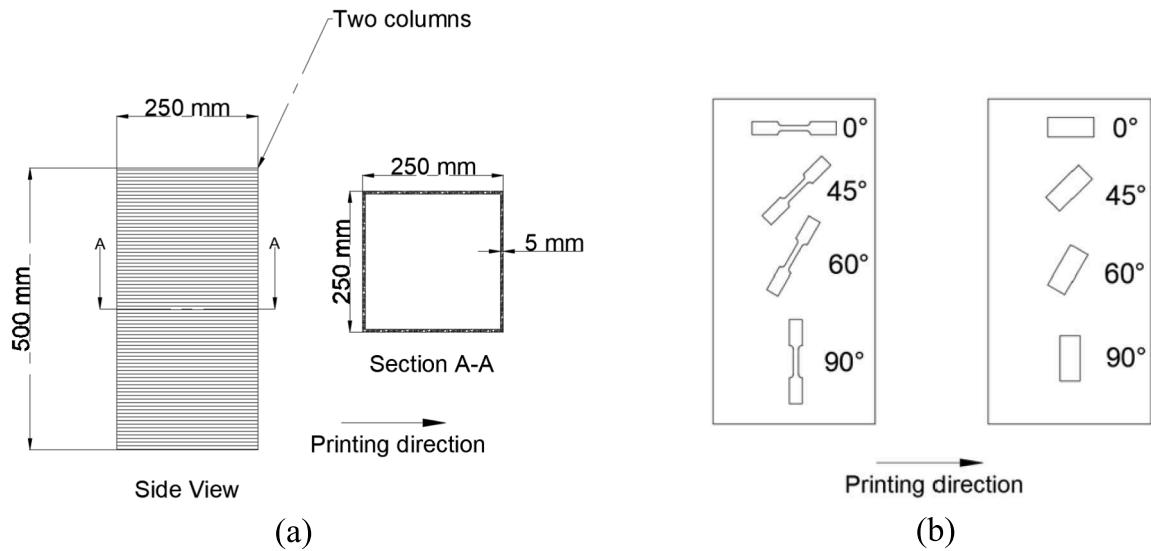
Fig. 2. The process of producing WAAM specimens: (a) parent material design, (b) extraction plan, (c) additive manufacturing via robotic cell, and (d) final parent material product.

Despite the growing body of research on WAAM components, studies on their integration with bolted connections remain limited. To date, as far as the authors are aware, four systematic investigations have examined double-lap configurations [18–21], while three studies have investigated single-lap configurations [22–24]. Notably, only one study has specifically investigated the inner plates of 316L stainless steel double-lap configurations, and it was limited to a single-bolt configuration [20]. This highlights the need for further research into the structural integrity and anisotropic nature of such plates.

Table 3

Printing parameters used during fabrication of tubular section specimens with WAAM.

Layers	Travel speed,(m/min)	Wire feed speed,(m/min)	Average Current, (A)	Average Voltage, (V)
1	0.45	8	225	13.5
2	0.60	6	188	12.5
3——250	0.78	6	188	12.5
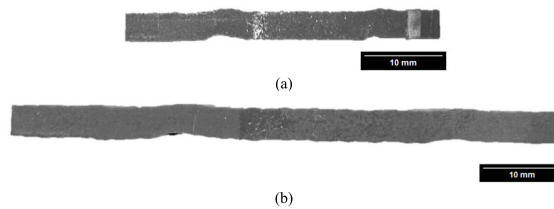
Fig. 3. Thickness, t variation in WAAM plates with extraction $\theta = 90°$ due to surface undulations: (a) view perpendicular to the breadth, b, and (b) view perpendicular to the length l.
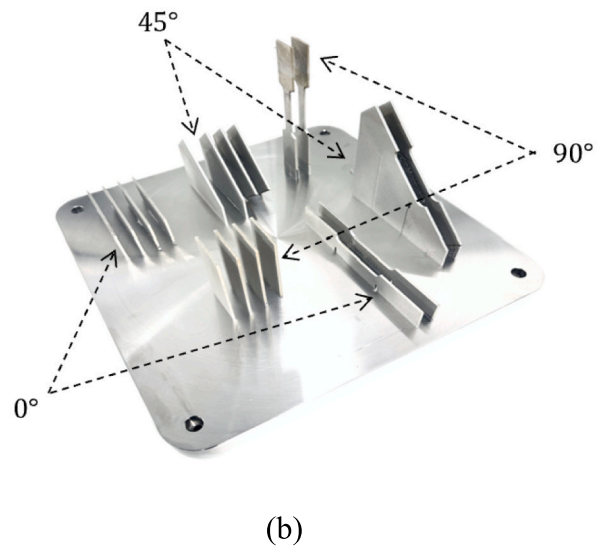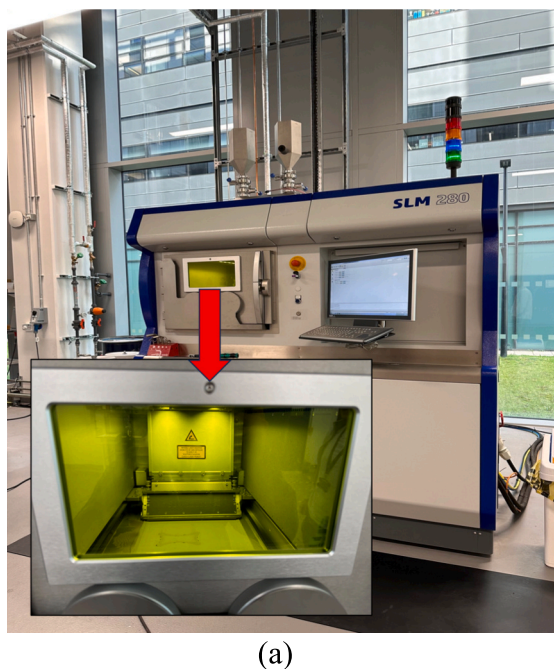
Fig. 4. SLM production process: (a) SLM 280 2.0® system with an arrow showing a zoom in to the powder bed, and (b) the final product, with indicating the printing direction, θ, before extraction.

Table 4

Printing parameters for SLM specimens.

Scanning region	Scanning strategy	Laser Power (W)	Scanning Speed (mm/s)	Stripe size (mm)	Hatch distance (mm)	Scan Rotation (°)
Volume (Hatching)	Stripe	250	950	7	0.1	0
Border	Single lines	150	450	—	—	—

The aforementioned studies have examined various bolt configurations, as-built and machined surfaces, interchangeable geometrical variables, and different extraction angles relative to the printing direction, θ, ranging from $0°$, $30°$, $45°$, $60°$ and $90°$. These studies have thoroughly demonstrated failure mechanisms in WAAM bolted connections. For instance, it was observed in [20] that the inner plates of 316L double-lap shear bolted connections with single-bolt configuration exhibited failures modes such as edge bearing (EB), net-section tensions (NST), Shear-out (SO), or a combination of two failure modes. Furthermore, the study revealed that print
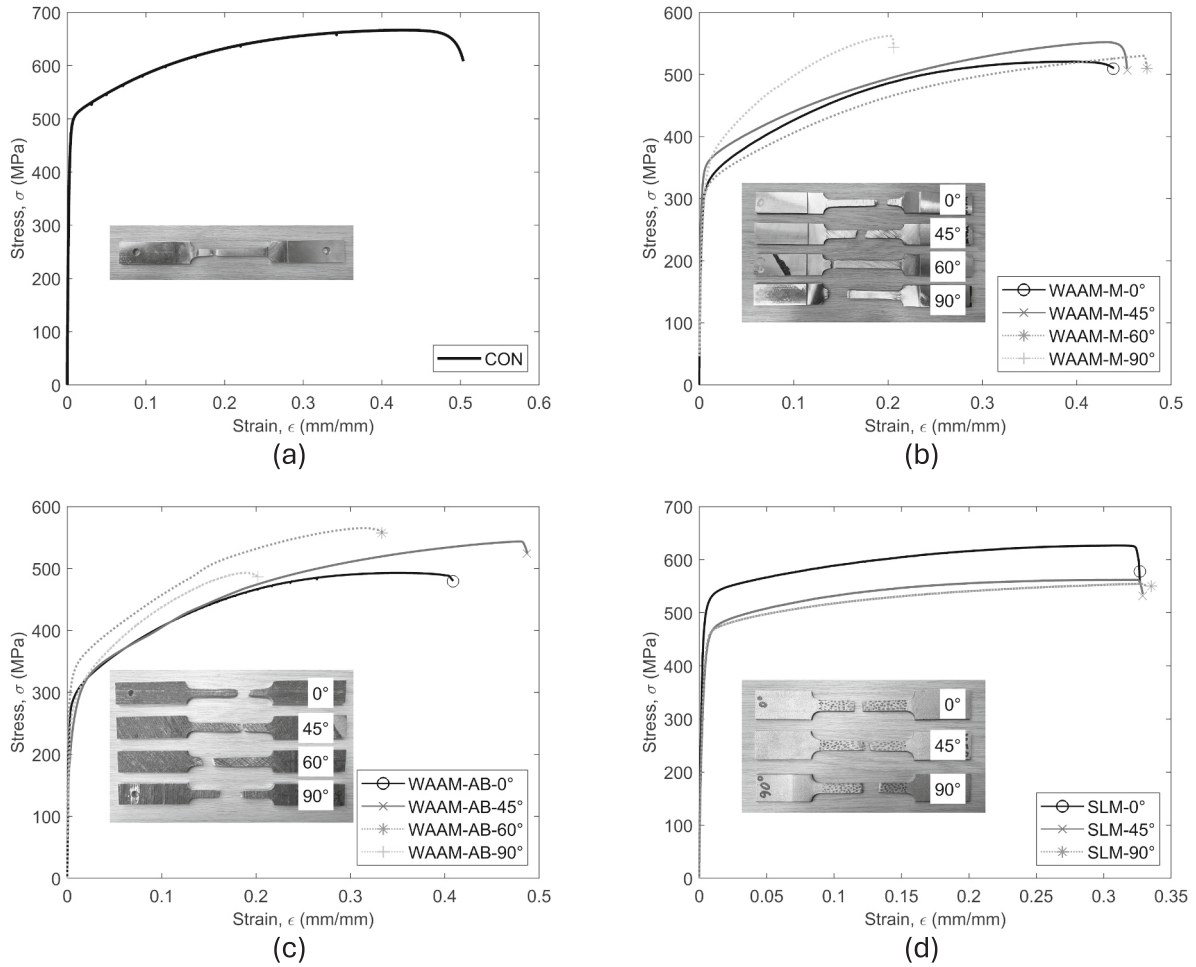
Fig. 5. 316L stainless steel test coupons stress–strain curves: (a) conventional, (b) WAAM-M, (C) WAAM-AB, and (D) SLM.

direction, θ had a minor influence, as machined and as-built plates exhibited the same failure modes despite a 10 % reduction in load-carrying capacity for the as-built plates. For clarity, Fig. 1 illustrates all possible failure modes for such connections, as defined by BS EN 1993–1-8 [25] and ANSI/AISC 370 [26] standards including bolt shear failure (BS) and block tearing (BT).

Building on the existing literature, this study aims to enhance the understanding of WAAM and SLM 316L stainless steel bolted connections by examining the failure and cracking behaviour of the inner plates in double-lap shear connections. It considers the effects of different surface conditions, print orientations, and both single- and double-bolt configurations. Additionally, the study investigates the influence of key geometrical parameters on failure mechanisms. In more detail, while a recent study investigated 316L stainless steel double-lap shear bolted connections [20], it was limited to WAAM-fabricated plates with a single-bolt configuration and did not include a comparative evaluation of different additive manufacturing technologies. To address this knowledge gap, the present paper systematically assesses and compares the performance of 316L stainless steel plates produced via both WAAM and SLM, considering both single- and double-bolt configurations. The findings presented here aim to provide researchers and practitioners with a more comprehensive understanding of how the manufacturing method and joint configuration influence failure mechanisms in bolted joints using additively manufactured plates.

2. Experimental work

2.1. Materials

The tested 316L stainless steel inner plates for the double-lap shear bolted connections were fabricated using three distinct methods: CON, WAAM, and SLM, while the outer, thicker plates were conventionally manufactured for all tests. Both the inner and outer CON plates were sourced from cold-rolled 316L stainless steel wrought sheets to ensure a smooth surface finish and serve as a reference.

Table 5
Summary of 316L stainless steel test coupons results.

Designation	Modulus of elasticity, E(GPa)	Offset yield stress, $\sigma_{0.2}$(MPa)	Ultimate stress, σ_u(MPa)	Strain at maximum stress, ε_u(mm/mm)	Fracture strain, ε_f(mm/mm)	Strain hardening exponent,n	Strength coefficient, K(MPa)	Yield ratio,$\sigma_{0.2}/\sigma_u$
CON	184	488	667	0.46	0.51	0.32	1211	0.73
WAAM-M-0°	143	288	521	0.39	0.44	0.34	1055	0.55
WAAM-M-45°	185	324	552	0.43	0.45	0.39	1166	0.59
WAAM-M-60°	160	297	530	0.47	0.47	0.41	1135	0.56
WAAM-M-90°	103	281	562	0.20	0.21	0.27	1025	0.50
WAAM-AB-0°	124	278	493	0.35	0.40	0.35	1012	0.56
WAAM-AB-45°	119	282	544	0.48	0.48	0.42	1181	0.52
WAAM-AB-60°	139	323	566	0.32	0.34	0.37	1193	0.57
WAAM-AB-90°	91	273	493	0.19	0.20	0.31	1002	0.55
SLM-AB-0°	160	520	627	0.31	0.32	0.25	1133	0.83
SLM-AB-45°	126	422	562	0.32	0.33	0.25	1014	0.75
SLM-AB-90°	120	419	554	0.33	0.33	0.26	1006	0.76

For the WAAM process, the materials used consisted of a 1.2 mm diameter 3Dprint AM 316L wire from Voestalpine Boehler and a carbon steel substrate plate measuring 295 × 295 × 29 mm. For the SLM process, the 316L powder was supplied by Nikon SLM Solutions and had a particle size of 10 – 45 μm, with a typical apparent density of 4.5 g/cm³. It was produced via gas atomisation with nitrogen. The 316L stainless steel substrate plate measured 278 × 278 × 25 mm Table.1 and Table.2 summarise the chemical composition and mechanical properties of the raw materials employed in the CON, SLM, and WAAM processes.

2.2. Manufacturing procedure

The fabrication of WAAM specimens involved four steps (see Fig. 2): first, designing a parent tubular section; second, planning the extraction based on the number of coupons and plates required; third, producing the tubular sections using a robotic welding cell; and finally, extracting the coupons and plates from the tubes from different directions, θ relative to the deposition direction, including 0°, 45°, 60° and 90°. A tubular parent specimen was selected because preliminary trials indicated that this type of build approach ensures more uniform cooling, thereby reducing residual stresses and distortions compared to the more commonly used single-bead linear walls. Two 250 × 250 mm tubular parent specimens were found adequate for extracting the desired number of inner plates.

The deposition of the samples was carried out by a KUKA KR 70 industrial robot arm equipped with a Fronius TransPuls Synergic 4000 CMT Power Source and a Robacta push–pull welding torch. The welding torch was oriented orthogonally to the travel direction, with a layer height set to 2 mm. The wire was deposited using a local argon shielding gas with a gas flow rate of 15 L/min, following specific printing parameters from Table.3. Initially, in the first two layers, due to the direct contact with the substrate plate, it was necessary to reduce the travel speed and increase the wire feed speed to increase the bead width and to ensure a consistent layer width throughout the sample. Furthermore, to allow the heat from the tube to dissipate, the deposition process was stopped every 25–50 layers to allow cleaning and cool-down of the welding torch, during which the tube was also allowed to cool down to room temperature naturally.

After production, the as-built plates were extracted using wire electrical discharge machining from the tubes with a final thickness, t varying around the nominal target of 5 mm (see Fig. 3 for plate length, l and breadth, b views), while the machined plates were milled down to 2 mm. This integrated approach to printing and extraction allowed us to minimise material waste.

The SLM specimens were produced using an SLM 280 2.0® system (Fig. 4a), which has a build volume of 280 × 280 × 365 mm. The material was deposited under a controlled atmosphere of Argon with a gas flow speed of 24 m/s, with a maximum oxygen level of 500 ppm and process pressure of 12 mbar. The build plate was kept at 100 °C during printing. The printing parameters used (Table.4) were those recommended by the original equipment manufacturer for a layer height of 50 μm. Additionally, the printing (scanning) direction after every layer was kept the same during the printing to understand the impact of the printing direction on sample orientation and the resulting effect on the mechanical anisotropy.

The SLM system offers a distinct advantage over WAAM because it fabricates specimens directly from CAD files with final dimensions similar to the original design file, including the desired printing direction, θ, requiring only extraction from the base plate and supports (Fig. 4b) depending on the application. To minimise edge distortions, solid supports were used to allow the sample being printed on the desired printing orientations relative to the build plate. Solid supports proved more effective than meshed ones during
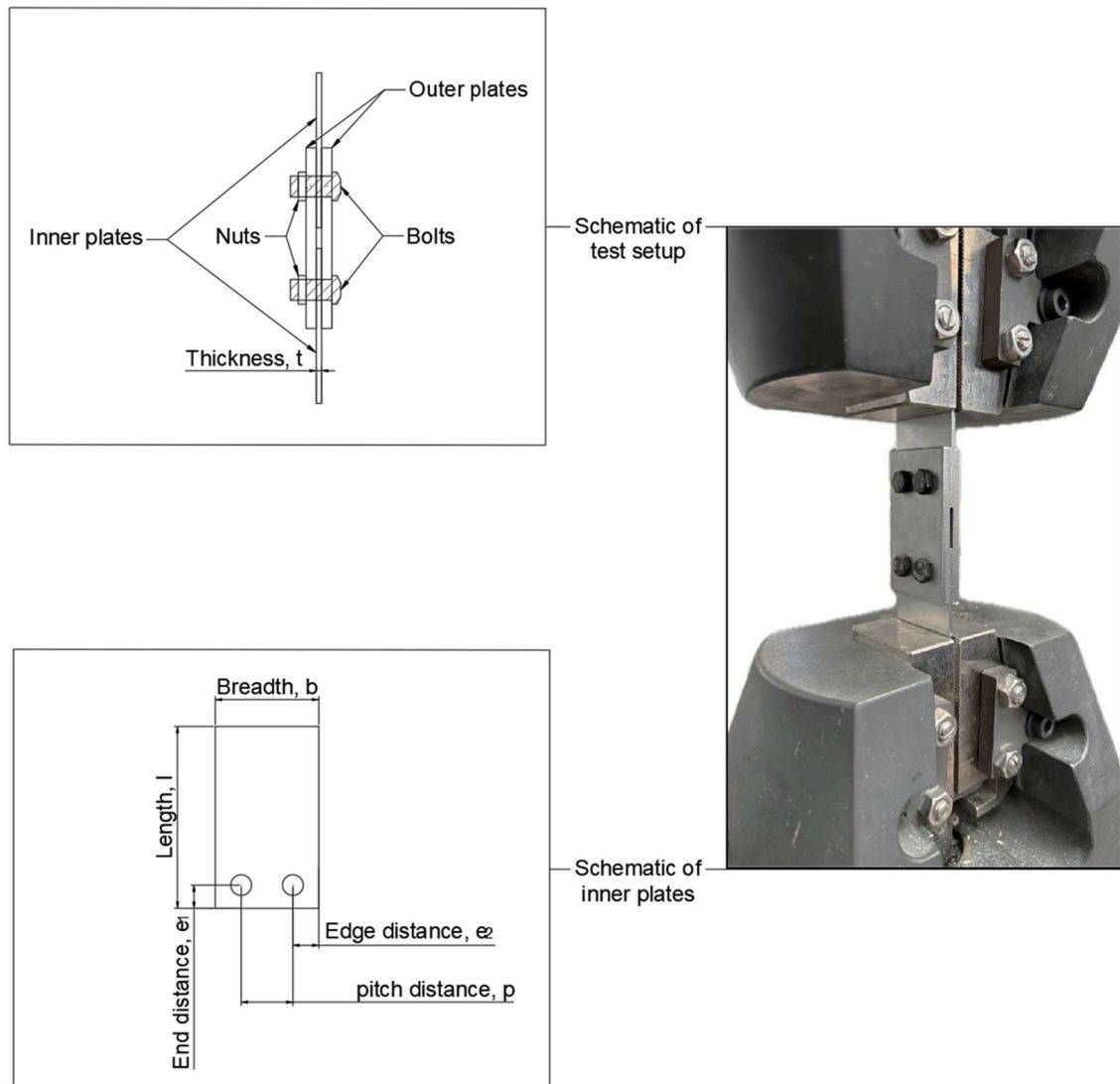
Fig. 6. Test setup for double-lap shear bolted connections, including schematics illustrating the test components and geometrical design variables of the inner plate, specifically for the double-bolted configuration.

trials to prevent part distortion and consequent damage between the interface of the support with the actual samples. The build preparation software Netfabb from Autodesk was used for orienting and positioning the samples and assigning the required printing parameters and supports.

After manufacturing, it was observed that the as-built SLM specimens exhibited a uniform noticeable surface roughness, R_a with an average value of 8 μm, according to the equipment specifications. Therefore, some plates were machined to remove the roughness and observe any possible variation of failure mechanism. Unlike the samples produced by WAAM, both the as-built and machined SLM plates were designed to maintain a consistent thickness, t of 2 mm.

2.3. Mechanical properties in standard test conditions

Prior to the bolted connections investigation, coupon uniaxial tensile tests were conducted on CON and AM metals at a displacement rate of 1 mm/min. The coupons design followed ASTM E8/E8M [27], adhering to the acceptable design thresholds for sub-size coupons. This allowed for the evaluation of the mechanical properties of AM metals in different extraction directions against the printing direction, θ under plain conditions. WAAM coupons were tested in four different extraction directions (θ = 0°, 45°, 60° and 90°) under both machined (WAAM-M) and as-built (WAAM-AB) conditions. As-built SLM coupons were tested in various orientations (θ = 0°, 45°, and 90°); the θ = 60° orientation was omitted due to production constraints. For SLM coupons the machined condition was excluded, as machining was shown not to impact the thickness, t of the specimen. Each coupon had a gauge breadth, b
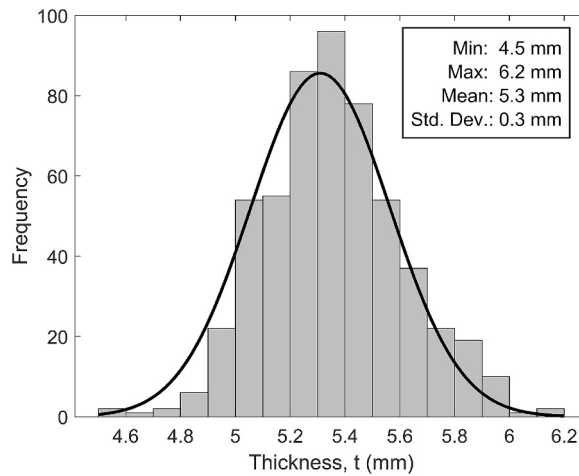
Fig. 7. Histogram of the measured thicknesses, t of all WAAM-AB inner plates along their breadth, b and length, l.
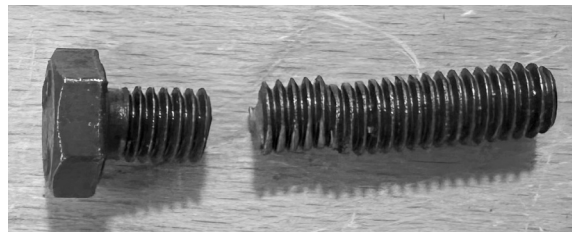

Fig. 8. BS failure of a grade 10.9 type M6 bolt as a result of increasing the thickness, t of the WAAM-AB inner plates.

and length, l of 8 mm and 38 mm, respectively. All specimens had t = 2 mm, except for the WAAM-AB coupons, which had a mean t = 5.3 mm.

As shown in the stress–strain curves (Fig. 5a,b,c,d) and summarised results in Table.5, the manufacturing process has a noticeable effect on the mechanical properties of the plain material. The CON coupons exhibited the highest ultimate tensile stress (σ_u = 667 MPa), highest fracture strain (ε_f = 0.51 mm/mm), and a relatively high strain hardening exponent (n = 0.32), indicating its superior ability to sustain plastic deformation before fracture. Among the WAAM coupons, orientation and surface condition played a critical role in mechanical response. WAAM-AB coupons exhibited lower modulus of elasticity, E values (ranging from 91 MPa to 139 MPa) compared to CON, WAAM-M, and SLM coupons. This reduction in stiffness can be attributed to possible inherited imperfections in the as-built condition, including micro voids, surface irregularities, and localised residual stresses. WAAM-M and WAAM-AB coupons extracted at $\theta = 45°$ and $60°$ exhibited slightly higher σ_u and ε_f, a behaviour is linked to the diagonal orientation of the slip planes during uniaxial tensile testing, which hinders slip activity and results in higher tensile stress [28]. However, for the WAAM-AB coupon at $\theta = 60°$, strain was lower due to variations in thickness, t and uneven surface condition along the gauge area. Additionally, both WAAM-M and WAAM-AB coupons at $\theta = 90°$ exhibited a significantly lower ε_f than all other coupons. This can be attributed to the load being applied perpendicular to the interlayer boundaries, making the coupon more susceptible to early crack initiation and lower overall ductility. The SLM coupons displayed the highest offset yield strength, $\sigma_{0.2}$ among all tested materials, with SLM-AB of $\theta = 0°$ reaching 520 MPa and maintaining a high yield ratio, $\sigma_{0.2}/\sigma_u$ with a value of 0.83, reflecting strong resistance to plastic deformation. However, with the exception of WAAM-M and WAAM-AB printed at $\theta = 90°$, the ε_f values for SLM coupons are lower than CON, and WAAM coupons, suggesting lower ductility despite their high strength. Furthermore, it is evident that the print direction, θ of SLM has less impact compared to WAAM coupons. These findings illustrate the influence of manufacturing method, surface condition, and material orientation on the structural integrity and mechanical performance of AM material.

2.4. Double-lap shear test design and setup

The test setup (Fig.6) consisted of double-lap shear connections designed to test the inner plates and minimise potential secondary bending during testing. Instead of using a typical axillary (spacer) plate at one end, both inner plates were directly connected to simulate a more realistic scenario. In all tests, both plates reached the ultimate load, with one plate failing completely. This behaviour was expected due to minor differences in material properties, fabrication tolerances, or bolt preload, which caused slight stress imbalances. Consequently, the failure mode presented in this study involves the complete failure of one inner plate. To ensure failure was confined to the inner plates, all outer plates were CON manufactured with increased thickness, t to provide additional stiffness and

Table 6
Design variables of produced inner plates for one-bolt configuration.

Designation	Bolt type	Bolt grade	Hole diameter,d_o	Thickness, t (mm)	End distance,e_1 (mm)	Edge distance,e_2 (mm)	Breadth,b (mm)
IP1-1-CON	M6	10.9	6.6	2	14	15	30
IP1-2-CON	M6	10.9	6.6	2	13	15	30
IP1-3-CON	M6	10.9	6.6	2	11	15	30
IP1-4-CON	M6	10.9	6.6	2	8	15	30
IP1-5-CON	M6	10.9	6.6	2	15	8	16
IP1-1-WAAM-M-0°	M6	10.9	6.6	2	14	15	30
IP1-1-WAAM-M-45°	M6	10.9	6.6	2	14	15	30
IP1-1-WAAM-M-60°	M6	10.9	6.6	2	14	15	30
IP1-1-WAAM-M-90°	M6	10.9	6.6	2	14	15	30
IP1-2-WAAM-M-0°	M6	10.9	6.6	2	14	15	30
IP1-2-WAAM-M-45°	M6	10.9	6.6	2	14	15	30
IP1-2-WAAM-M-60°	M6	10.9	6.6	2	14	15	30
IP1-2-WAAM-M-90°	M6	10.9	6.6	2	14	15	30
IP1-3-WAAM-M-0°	M6	10.9	6.6	2	11	15	30
IP1-4-WAAM-M-0°	M6	10.9	6.6	2	8	15	30
IP1-1-WAAM-AB-0°	M8	12.9	8.4	5.4	14	15	30
IP1-2-WAAM-AB-0°	M8	12.9	8.4	5.4	13	15	30
IP1-2-WAAM-AB-45°	M8	12.9	8.4	5.3	13	15	30
IP1-2-WAAM-AB-60°	M8	12.9	8.4	5.2	13	15	30
IP1-2-WAAM-AB-90°	M8	12.9	8.4	5.2	13	15	30
IP1-3-WAAM-AB-0°	M8	12.9	8.4	5.3	11	15	30
IP1-4-WAAM-AB-0°	M8	12.9	8.4	5.4	8	15	30
IP1-5-WAAM-AB-0°	M8	12.9	8.4	5.2	15	8	16
IP1-5-WAAM-AB-45°	M8	12.9	8.4	5.4	15	8	16
IP1-5-WAAM-AB-60°	M8	12.9	8.4	5.3	15	8	16
IP1-5-WAAM-AB-90°	M8	12.9	8.4	5.3	15	8	16
IP1-1-SLM-M-0°	M6	10.9	6.6	2	14	15	30
IP1-1-SLM-AB-0°	M6	10.9	6.6	2	14	15	30
IP1-2-SLM-AB-0°	M6	10.9	6.6	2	13	15	30
IP1-2-SLM-AB-45°	M6	10.9	6.6	2	13	15	30
IP1-2-SLM-AB-90°	M6	10.9	6.6	2	13	15	30
IP1-5-SLM-AB-0°	M6	10.9	6.6	2	15	8	16
IP1-5-SLM-AB-45°	M6	10.9	6.6	2	15	8	16
IP1-5-SLM-AB-90°	M6	10.9	6.6	2	15	8	16

prevent unintended failures and minimise deformations. The plates were connected by high-strength 10.9, fully threaded M6 bolts to eliminate possibility of shear failure. For proper assembly, a medium fit 0.6 mm hole clearance was chosen based on IS0 273 [29]. The tested plates featured two main configurations: single-bolted and double-bolted. As with the coupon design, the plates were intentionally kept relatively small to maximise the number of specimens produced while adhering to the printing limitations of WAAM and SLM. In both single- and double-bolt configurations, critical design geometrical parameters serve as the key variables affecting the plates' failure loads and modes [25]. These geometrical variables included end distance, e_1, edge distance, e_2, breadth, b, and pitch distance, (p). Variations in these variables, along with changes in surface condition and print orientation, were introduced to promote the occurrence of specific failure modes, thereby enhancing our understanding of the behaviour of the AM printed plates. It should be noted that the inner plate thickness, t was maintained at 2 mm for CON, WAAM-M, SLM-AB, and SLM-M specimens, while it varied for WAAM-AB specimens with a mean t = 5.3 mm (similar to WAAM-AB coupons), which closely matches to the nominal target of t = 5 mm (Fig.7). Similar to the coupon tests, the double-lap shear tests were performed at a displacement rate of 1 mm/min.

Due to the increased thickness, t of WAAM-AB plates and the corresponding enlargement of the outer plates, standard design estimations and experimental trials confirmed that the bolt specifications should be upgraded to a grade 12.9 bolt with a non-threaded M8 configuration. A close fit hole clearance of 0.4 mm was selected to account for the absence of bolt threads. This adjustment was implemented to prevent the bolt shear (BS) failure, which was observed during preliminary trials (see Fig.8). Although increasing the bolt size required enlarging the hole diameter, d_o, all other variables such as end distance, e_1, edge distance, e_2, and pitch distance, p were kept unchanged to assess whether the failure mode remained consistent. As a result, these variables in most WAAM-AB plates were slightly below the minimum requirements specified in BS EN 1993–1-8 [25], where $e_1, e_2 = 1.2d_o$ and $p = 2.4d_o$. However, they remained withing 20 % to these recommended values, expect one specimen where it reached 30 %. For instance, with a hole diameter of 8.4 mm, a minimum end distance, e_1 would be approximately 10 mm, whereas the actual distance used was 8 mm, representing a

Table 7
Design variables of produced inner plates for two-bolt configuration.

Designation	Bolt type	Bolt grade	Hole diameter, d_o	Thick-ness, t (mm)	End distance, e_1 (mm)	Edge distance, e_2 (mm)	Pitch distance, p (mm)	Breadth, b (mm)
IP2-1-CON	M6	10.9	6.6	2	12	12	16	40
IP2-2-CON	M6	10.9	6.6	2	11	12	16	40
IP2-3-CON	M6	10.9	6.6	2	8.2	12	16	40
IP2-4-CON	M6	10.9	6.6	2	8	12	16	40
IP2-5-CON	M6	10.9	6.6	2	7	12	16	40
IP2-6-CON	M6	10.9	6.6	2	16	8	24	40
IP2-7-CON	M6	10.9	6.6	2	15	11	18	40
IP2-1-WAAM-M-0°	M6	10.9	6.6	2	12	12	16	40
IP2-1-WAAM-M-45°	M6	10.9	6.6	2	12	12	16	40
IP2-1-WAAM-M-60°	M6	10.9	6.6	2	12	12	16	40
IP2-1-WAAM-M-90°	M6	10.9	6.6	2	12	12	16	40
IP2-2-WAAM-M-0°	M6	10.9	6.6	2	11	12	16	40
IP2-3-WAAM-M-0°	M6	10.9	6.6	2	8.2	12	16	40
IP2-3-WAAM-M-45°	M6	10.9	6.6	2	8.2	12	16	40
IP2-3-WAAM-M-60°	M6	10.9	6.6	2	8.2	12	16	40
IP2-3-WAAM-M-90°	M6	10.9	6.6	2	8.2	12	16	40
IP2-4-WAAM-M-0°	M6	10.9	6.6	2	8	12	16	40
IP2-5-WAAM-M-0°	M6	10.9	6.6	2	7	12	16	40
IP2-7-WAAM-M-0°	M6	10.9	6.6	2	8.2	12	16	40
IP2-2-WAAM-AB-0°	M8	12.9	8.4	5.5	11	12	16	40
IP2-3-WAAM-AB-0°	M8	12.9	8.4	5.6	8.2	12	16	40
IP2-3-WAAM-AB-45°	M8	12.9	8.4	5.2	8.2	12	16	40
IP2-3-WAAM-AB-60°	M8	12.9	8.4	5.5	8.2	12	16	40
IP2-3-WAAM-AB-90°	M8	12.9	8.4	5.3	8.2	12	16	40
IP2-4-WAAM-AB-0°	M8	12.9	8.4	5.0	8	12	16	40
IP2-5-WAAM-AB-0°	M8	12.9	8.4	5.3	7	12	16	40
IP2-6-WAAM-AB-0°	M8	12.9	8.4	5.4	16	8	24	40
IP2-6-WAAM-AB-45°	M8	12.9	8.4	5.0	16	8	24	40
IP2-6-WAAM-AB-60°	M8	12.9	8.4	5.3	16	8	24	40
IP2-6-WAAM-AB-90°	M8	12.9	8.4	5.0	16	8	24	40
IP2-7-WAAM-AB-0°	M8	12.9	8.4	5.4	8.2	12	16	40
IP2-7-SLM-M-0°	M6	10.9	6.6	2	15	11	18	40
IP2-6-SLM-AB-0°	M6	10.9	6.6	2	16	8	24	40
IP2-6-SLM-AB-45°	M6	10.9	6.6	2	16	8	24	40
IP2-6-SLM-AB-90°	M6	10.9	6.6	2	16	8	24	40
IP2-7-SLM-AB-0°	M6	10.9	6.6	2	15	11	24	40

IP1-1-CON	IP1-1-WAAM-M-0°	IP1-1-WAAM-M-45°

IP1-1-WAAM-M-60°	IP1-1-WAAM-M-90°	IP1-1-WAAM-AB-0°

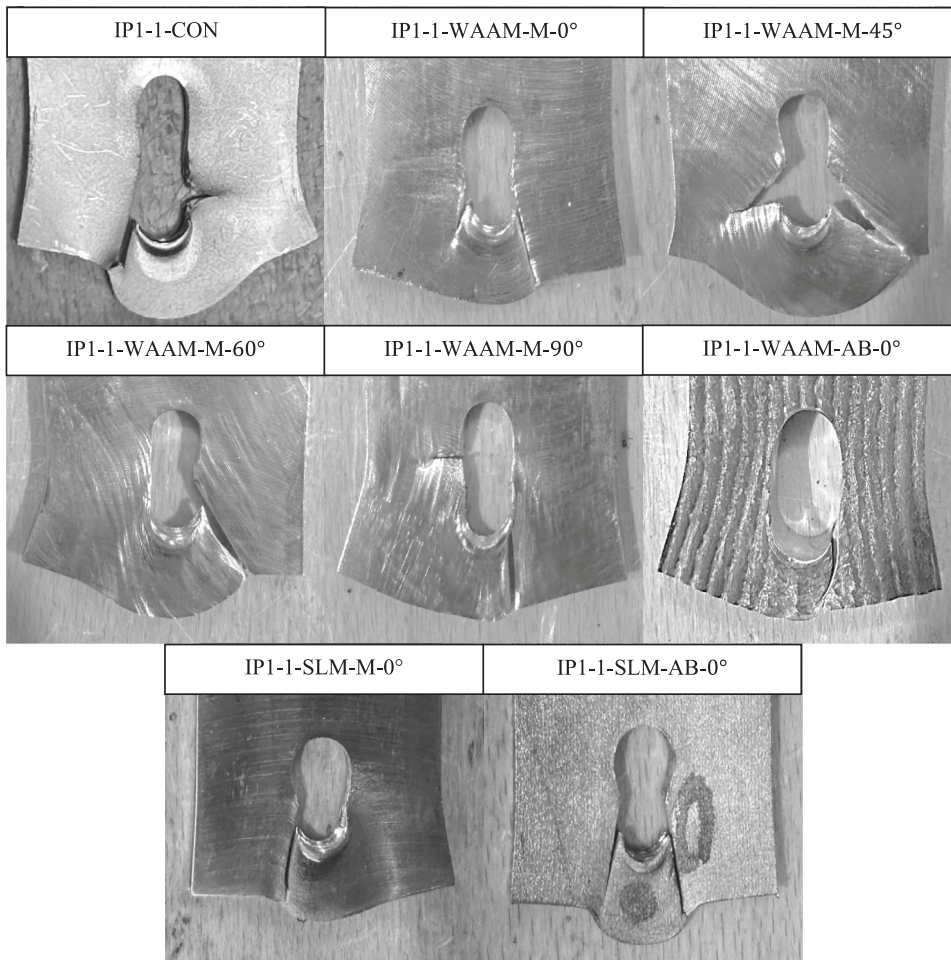| IP1-1-SLM-M-0°	IP1-1-SLM-AB-0°

Fig. 9. Failure modes for IP1-1 configuration of CON and AM plates.

small deviation from the standards. Experimental tests confirmed that these minor deviations had a negligible impact on the failure mode of the inner plates.

Table6 and Table.7 present the design variables of the produced inner plates for the one-bolt and two-bolt configurations, respectively. Each inner plate is uniquely designated to indicate its configuration and manufacturing process. The notation (IP) refers to an inner plate, with plates featuring a one-bolt configuration labelled (IP1) and those with a two-bolt configuration labelled (IP2). The number following IP1 or IP2 (e.g., in IP1-1) represents the specimen number, which corresponds to a unique set of geometrical variables such as end distance, e_1, edge distance, e_2, and breadth, b. For specimens produced via AM, the designation also includes the surface condition and the extraction or printing angle. In this context, (M) indicates that the surface was machined either to achieve the specified thickness, t for WAAM or to remove the surface roughness in SLM, while (AB) denotes an as-built condition. Finally, the last number specifies the angle of printing/extraction. For example, the designation IP1-1-WAAM-M-0° identifies an inner plate produced using WAAM with a one-bolt configuration, specimen number 1, where M signifies that the surface was machined to achieve t = 2 mm, with the angle of printing/extraction of $\theta = 0°$. Although one inner plate in the WAAM-AB specimen experienced total failure, the mean thickness, t reported is based on both plates, as each contributed to the load-bearing capacity prior to rupture.

3. Effect of the manufacturing method on load capacity

For single-bolt configurations, the experimental loads of WAAM and SLM tests were compared to their respective CON counterparts for each test geometry. WAAM-M tests generally exhibited comparable performance with variations ranging from a reduction of 10.5 % in IP1-2-WAAM-M-90° to a modest increase of 5.0 % in IP1-2-WAAM-M-45°. SLM tests, both machined and as-built, exhibited variations generally within ±5 %, with a few cases showing reductions of up to 10.8 % compared to their CON counterparts. Although the WAAM-AB tests appeared to yield significantly higher failure loads, in some cases more than double the CON values, such as a 136 % increase in IP1-1-WAAM-AB-0°, these increases are attributed to their greater thickness and are therefore not directly comparable to the 2 mm thick tests in terms of load capacity.
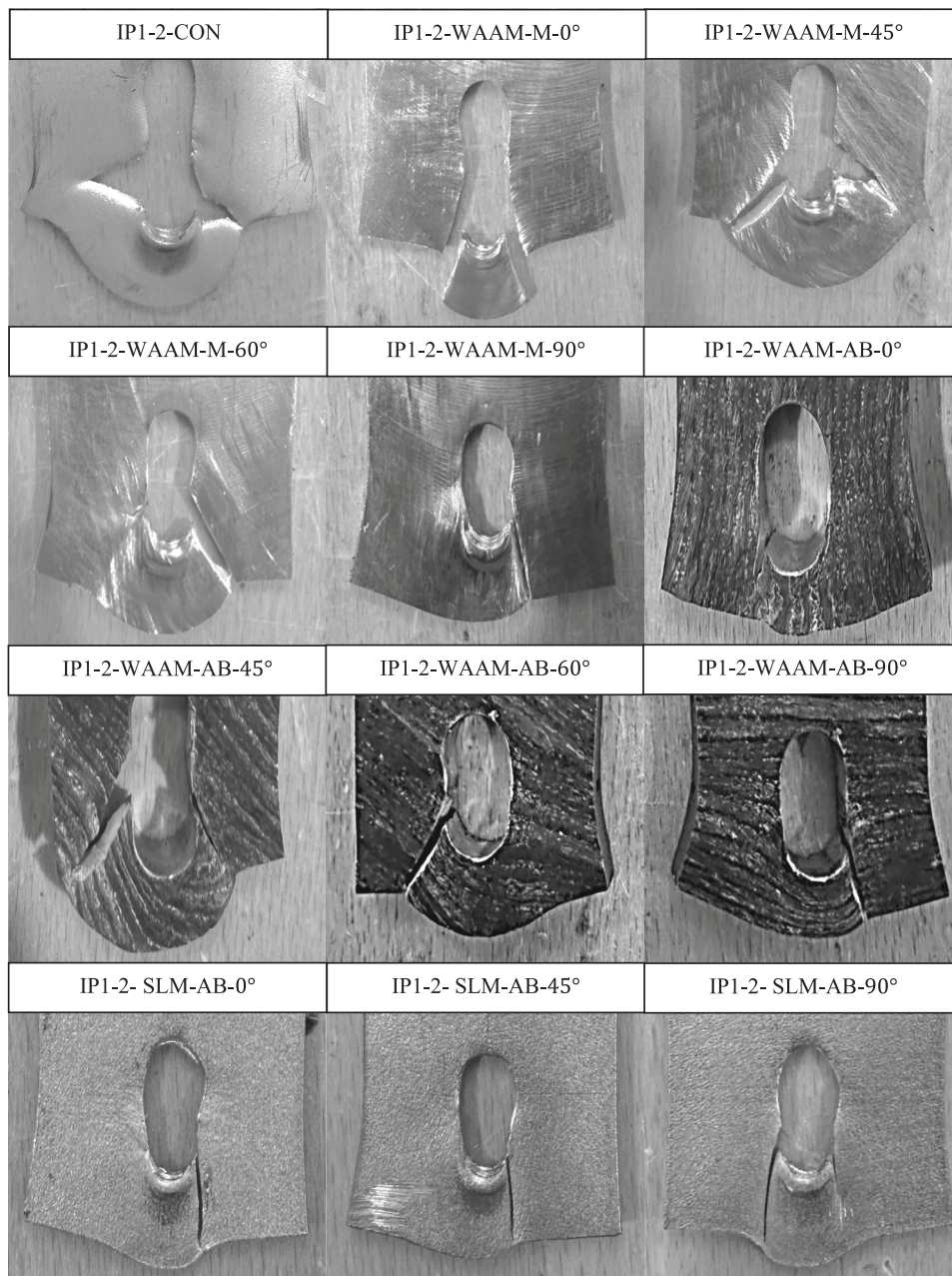
IP1-2-CON	IP1-2-WAAM-M-0°	IP1-2-WAAM-M-45°

IP1-2-WAAM-M-60°	IP1-2-WAAM-M-90°	IP1-2-WAAM-AB-0°

IP1-2-WAAM-AB-45°	IP1-2-WAAM-AB-60°	IP1-2-WAAM-AB-90°

IP1-2- SLM-AB-0°	IP1-2- SLM-AB-45°	IP1-2- SLM-AB-90°

Fig. 10. Failure modes for IP1-2 configuration of CON and AM plates.

For double-bolt configurations, WAAM-M tests showed small variations, with the largest reduction being 7.3 % in IP2-1-WAAM-M-90° and a minor increase of 5.6 % in IP2-3-WAAM-M-45°. SLM tests also exhibited variations within ±5 % of the corresponding CON values. The WAAM-AB tests displayed noticeable increases in failure load, with IP2-6-WAAM-AB-0° showing the highest increase at 133 %, relative to its CON counterpart. Nonetheless, when the comparison is restricted to tests with consistent thickness, the differences in load capacity across all manufacturing methods are not significant.

4. Failure mode and crack behaviour of the plates

4.1. Single-bolt configuration

The investigation on failure modes and crack behaviour across both conventional and AM approaches was conducted through visual observation of the completely failed test plates. Starting with the single-bolt configurations, Fig.9 that represents IP1-1 shows
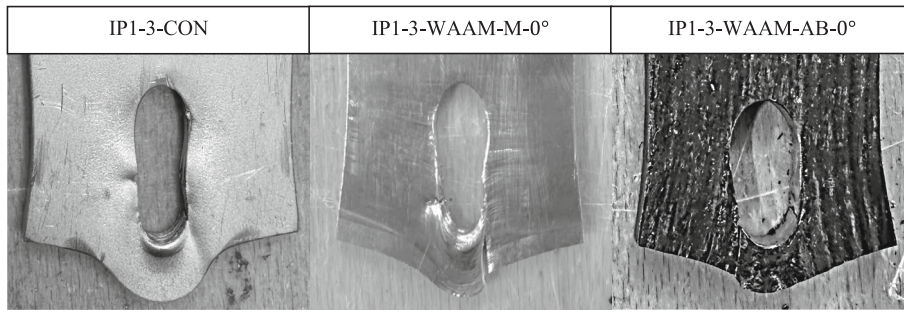
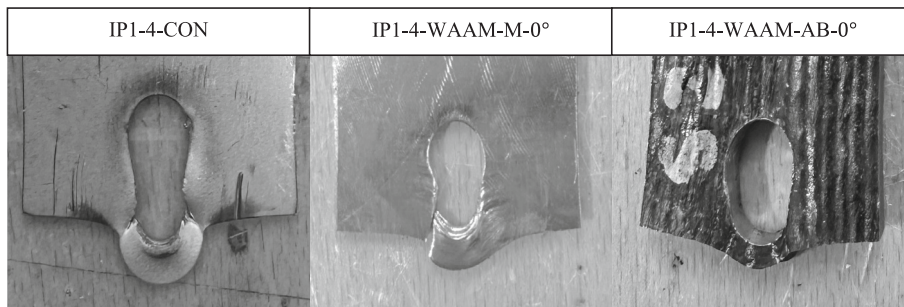**Fig. 11.** Failure modes for IP1-3 configuration of CON and AM plates.

Fig. 12. Failure modes for IP1-4 configuration of CON and AM plates.

that all plates failed due to a combined EB and SO, primarily induced by a relatively small end distance, e_1 in the bolted connection. The deformation around the hole indicates that localised bearing stresses led to a significant plasticity before final failure. This is evident from the compressed and plastically deformed region at the bottom edge of the hole, where the bolt exerted high contact pressure. Additionally, a distinct crack at the hole edge observed in IP1-1-CON and IP1-1-WAAM-M-90°, suggesting that the shear-induced hole elongation let to a tensile stress concentration in this region, in turn resulting in early micro-cracking and crack initiation. In most cases, SO crack extended from the hole along e_1, following a straight tearing path. Notably, the curved nature of the crack in IP1-1-WAAM-M-45° and IP1-1-WAAM-M-60° suggests secondary tensile effects, possibly influenced by the layered structure of WAAM, which may altered crack propagation behaviour to be diagonal. Similarly, Fig.10, representing the IP1-2 configuration, exhibited a combined failure mode of EB and SO. However, in the IP1-2-CON plate, crack propagation along the breadth was more pronounced, suggesting that manufacturing-induced anisotropy in the CON material may have contributed to guiding the crack path. This contrasts with the WAAM specimens, where the layered structure and its orientation were the governing factors affecting crack propagation. Despite the increased thickness, t and hole diameter, d_o, WAAM-AB plates exhibited the same failure mode and crack behaviour as the other CON and AM plates. Alongside the observed load bearing capacity results of experimental tests, this outcome suggests that unlike other geometric parameters (e.g., e_1, e_2, and b), the thickness, t has larger effects on the final failure capacity than on the failure mode. As e_1 decreases, the failure modes observed in Fig.11 and Fig.12 remained similar to those shown in the earlier figures, though SO failure was more pronounced. In Fig.13, the significantly smaller plate breadth, b resulted in a NST failure mode. Cracks initiated at one edge of the bolt hole and propagated directly to the plate boundary, a behaviour observed consistently across all IP1-5 plates, except for the CON plates, where crack propagation remained incomplete. However, no notable differences were observed in crack initiation or propagation paths, highlighting the dominant influence of the reduced breadth, b on the NST failure mechanism.

4.2. Double-bolt configuration

For the double-bolt configurations, failure in both CON and AM plates was investigated under varying geometrical conditions, including varying pitch distance, p between the centres of the bolt holes. As shown in Fig.14, the small value of p promoted crack initiation between the holes, resulted in a combined of EB and the onset of partial BT failure modes for the IP2-1-CON and IP2-1-WAAM-M-0° plates, while in all other plates the partial BT crack propagated further. Similar to the single-bolt configuration, crack propagation in the WAAM-M plates was influenced by the printing layered structure, with diagonal crack paths observed in the IP2-1-WAAM-M-45° and IP2-1-WAAM-M-60° specimens Fig. 15 shows that a slight decrease in e_1 relative to IP1-1 plates did not alter the failure mode of IP2-2-CON and IP2-2-WAAM-AB-0°. However, a complete BT failure was observed in IP2-2-WAAM-M-0°. This can be attributed to the combined effect of tension cracking across the net section between the holes and shear cracking along the hole edges. As shown in Fig.16 and Fig.17 for the IP2-3 and IP2-4 plates, further reductions in e_1, resulted in failure modes consisting of either EB combined with complete BT or EB combined with SO. Next, Fig.18 illustrates that the IP2-5 plates, which had the smallest e_1,
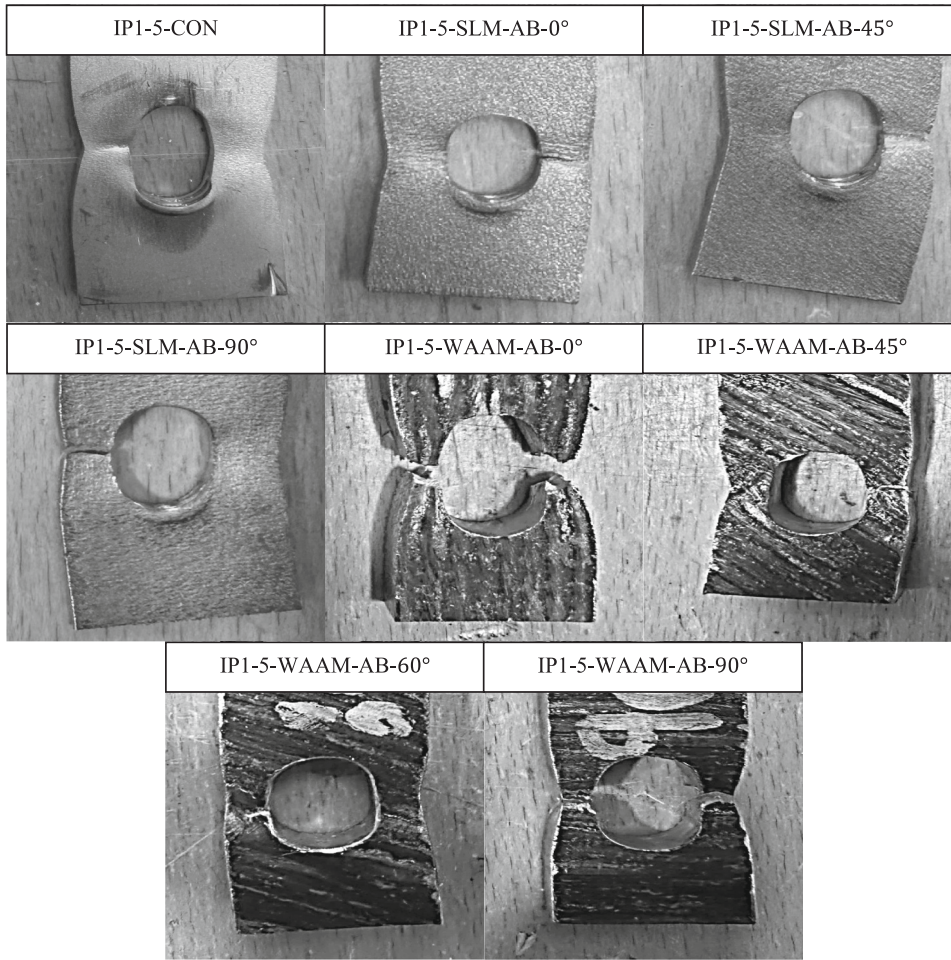
Fig. 13. Failure modes for IP1-5 configuration of CON and AM plates.

underwent exclusively EB and SO failures. Hence, for double-bolt configuration, as e_1 decreases, the failure mode transitions from partial BT to either EB combined with complete BT or EB combined with SO, emphasising the critical role of this variable in driving the progression toward shear-dominated failures. Subsequently, Fig.19 examines the influence of increasing p, which in turn reduces e_2, causing the failure to shift toward EB and partial NST along the edges. This behaviour was consistently observed across both CON and AM plates, indicating that p can significantly influence crack initiation and propagation. Finally, Fig.20 shows that providing sufficient e_1 and p led to EB and initiation of partial BT in all plates, except for IP2-7-WAAM-AB-0°, where complete NST failure was occurred. This exceptional failure could be attributed to manufacturing defects inherent to the WAAM process highlighting the significant influence of manufacturing procedures on overall failure modes.

CON and AM plates exhibited broadly similar failure modes and crack patterns. However, a detailed analysis of the WAAM machined and as-built plates extracted at $\theta = 45°$ and $60°$ revealed distinct crack paths. This highlights the complex interplay of geometric and manufacturing factors in determining the failure process. Although these subtle differences in crack propagation are noteworthy, they do not result in a fundamentally different overall failure mode between the CON and AM plates.

5. Conclusions

Based on the mechanical behaviour of CON and AM 316L stainless steel coupons, as well as the failure modes in single- and double-bolted configurations of hybrid double-lap shear connections, the following conclusions were drawn:

a) CON coupon exhibited superior tensile properties, achieving the highest σ_u and ε_f, whereas WAAM specimens showed clear sensitivity to surface condition and extraction orientation, exhibiting improved properties at $\theta = 60°$ and $45°$ but significantly reduced ductility at $\theta = 90°$. Meanwhile, SLM coupons achieved the highest $\sigma_{0.2}$ and yield ratio but exhibited notably low ductility, though still exceeding that of WAAM specimens extracted at $\theta = 90°$.
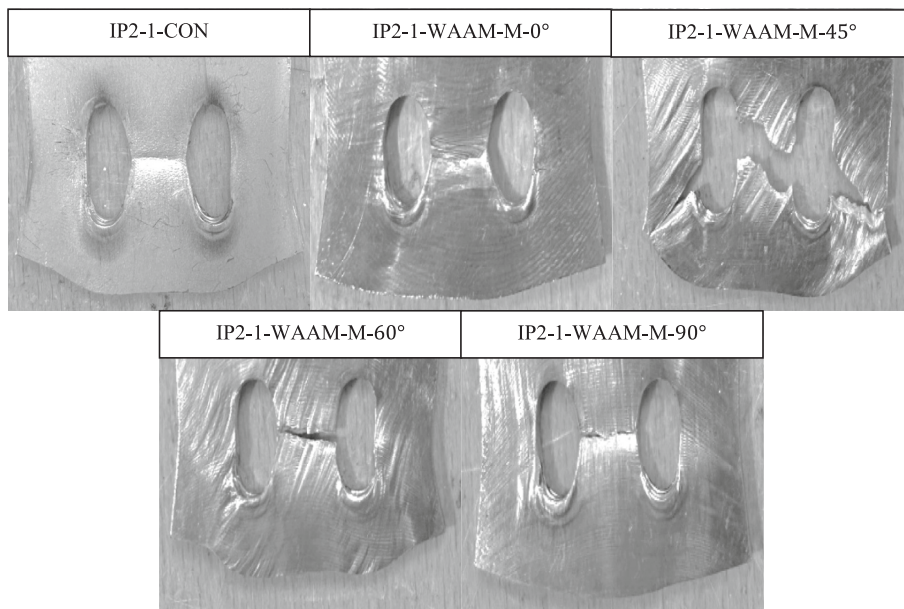
IP2-1-CON	IP2-1-WAAM-M-0°	IP2-1-WAAM-M-45°

IP2-1-WAAM-M-60°	IP2-1-WAAM-M-90°

Fig. 14. Failure modes for IP2-1 configuration of CON and AM plates.

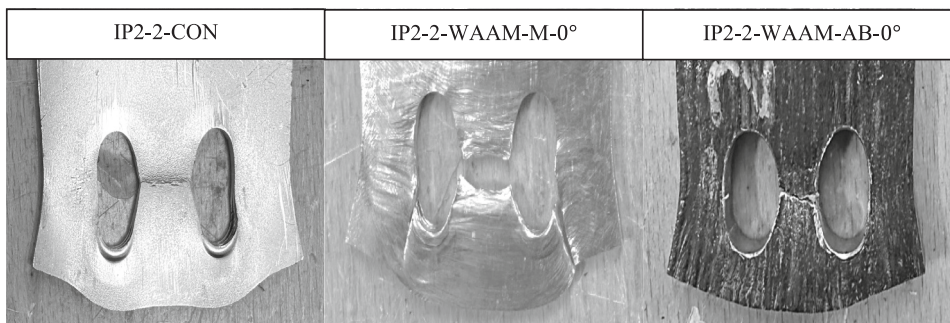| IP2-2-CON	IP2-2-WAAM-M-0°	IP2-2-WAAM-AB-0°

Fig. 15. Failure modes for IP2-2 configuration of CON and AM plates.

b) When the thickness is comparable, the load capacity of WAAM-M and SLM tests closely aligns with that of CON specimens, indicating that manufacturing method does not significantly affect global load-bearing performance.

c) Variations in geometric variables, such as e_1, e_2, b and p, predominantly influence the failure behaviour, reinforcing their critical role in the design of inner plates for double-lap bolted connections.

d) Crack initiation and propagation modes were broadly similar among CON and AM plates; however, WAAM machined and as-built plates extracted at $\theta = 45°$ and $60°$ displayed unique crack paths influenced by their layered microstructure and surface undulation, with cracks propagating diagonally relative to the loading direction. In contrast, SLM specimens maintain consistent behaviour with minimal sensitivity to the surface condition and print orientation.

e) Overall, the majority of AM plates achieved similar failure modes to their CON counterparts. This demonstrates that selecting optimal printing orientations and standardised geometrical design variables can ensure reliable structural performance in hybrid 316L stainless steel double-lap shear connections incorporating AM metals.

f) While the present study focuses on the mechanical and failure behaviour aspects, further work is needed to establish a complete Process-Structure-Property-Performance (PSPP) relationship for the additively manufactured metals considered, with particular emphasis placed on grain morphology, texture, and anisotropy.

CRediT authorship contribution statement

Hasan Almuhanna: Writing – original draft, Investigation, Formal analysis. **Giacomo Torelli:** Writing – review & editing, Supervision. **Renan Kindermann:** Writing – review & editing. **Luca Susmel:** Writing – review & editing, Supervision, Methodology, Conceptualization.
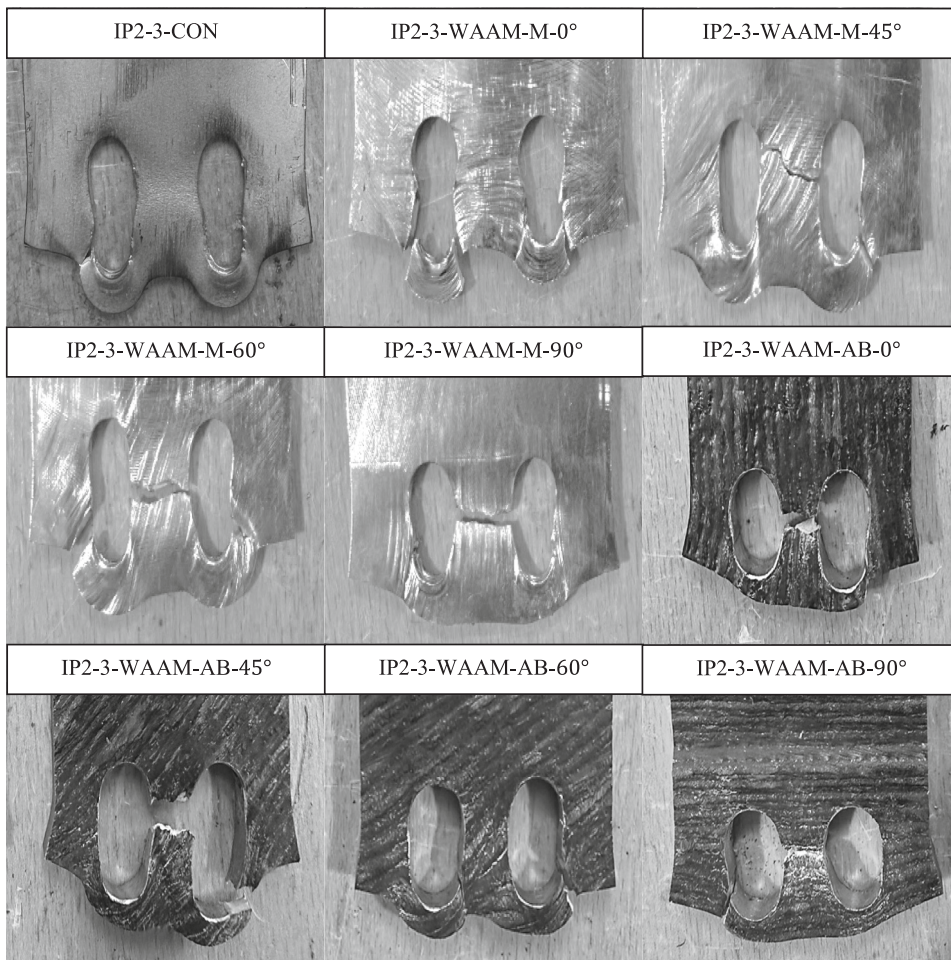
IP2-3-CON	IP2-3-WAAM-M-0°	IP2-3-WAAM-M-45°

IP2-3-WAAM-M-60°	IP2-3-WAAM-M-90°	IP2-3-WAAM-AB-0°

IP2-3-WAAM-AB-45°	IP2-3-WAAM-AB-60°	IP2-3-WAAM-AB-90°

Fig. 16. Failure modes for IP2-3 configuration of CON and AM plates.

IP2-4-CON	IP2-4-WAAM-M-0°	IP2-4-WAAM-AB-0°
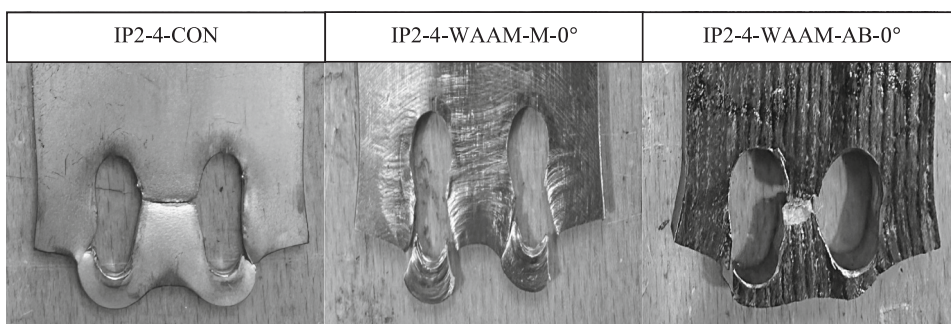
Fig. 17. Failure modes for IP2-4 configuration of CON and AM plates.

IP2-5-CON	IP2-5-WAAM-M-0°	IP2-5-WAAM-AB-0°

Fig. 18. Failure modes for IP2-5 configuration of CON and AM plates.

IP2-6-CON	IP2-6-WAAM-AB-0°	IP2-6-WAAM-AB-45°
IP2-6-WAAM-AB-60°	IP2-6-WAAM-AB-90°	IP2-6-SLM-AB-0°
	IP2-6-SLM-AB-45°	IP2-6-SLM-AB-90°

Fig. 19. Failure modes for IP2-5 configuration of CON and AM plates.

IP2-7-CON	IP2-7-WAAM-M-0°	IP2-7-WAAM-AB-0°

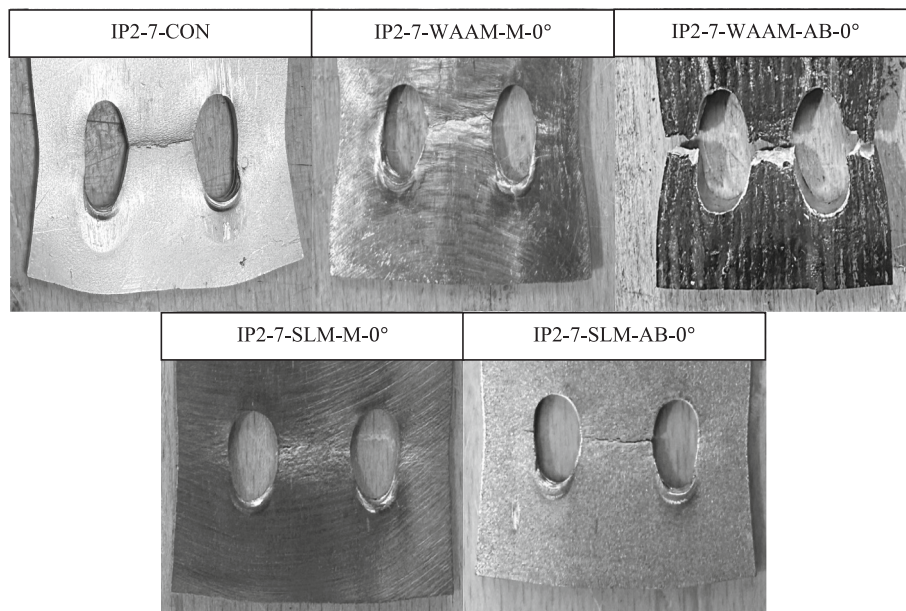| IP2-7-SLM-M-0°	IP2-7-SLM-AB-0°
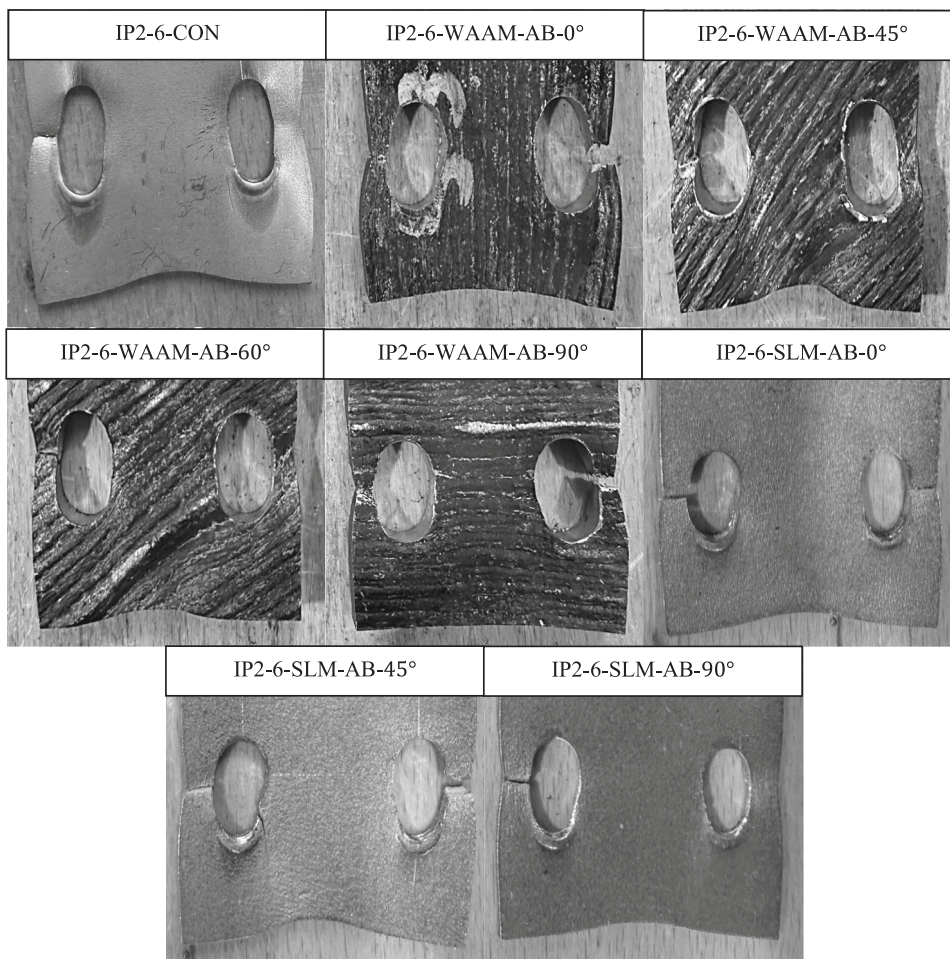
Fig. 20. Failure modes for IP2-7 configuration of CON and AM plates.

Declaration of competing interest

The authors declare that they have no known competing financial interests or personal relationships that could have appeared to influence the work reported in this paper.

Acknowledgment

Data availability

Data will be made available on request.

References

[1] C. Brogan, World's first 3D-printed steel footbridge unveiled by Queen Máxima in Amsterdam, Imperial College, London, 2021.
[2] T. Feucht, B. Waldschmitt, J. Lange, M. Erven, 3D-Printing with Steel: Additive Manufacturing of a Bridge in situ, (2021) 1695–1701. https://doi.org/10.1002/cepa.
[3] C. Buchanan, L. Gardner, Metal 3D printing in construction: A review of methods, research, applications, opportunities and challenges, Eng Struct 180 (2019) 332–348. https://doi.org/10.1016/j.engstruct.2018.11.045.
[4] BS EN ISO/ASTM 52900, Additive manufacturing General principles Fundamentals and vocabulary, 2021.
[5] ASTM F3187-16, Guide for Directed Energy Deposition of Metals, 2023. https://doi.org/10.1520/F3187-16R23.
[6] A. Astarita, G. Campatelli, P. Corigliano, G. Epasto, F. Montevecchi, F. Scherillo, G. Venturini, Microstructure and mechanical properties of specimens produced using the wire-arc additive manufacturing process, Proc Inst Mech Eng C J Mech, Eng Sci 235 (2021) 1788–1798, https://doi.org/10.1177/0954406219883324.
[7] Y. Ayan, N. Kahraman, Wire Arc Additive Manufacturing of Low-Carbon Mild Steel Using Two Different 3D Printers, Phys. Met. Metall. 122 (2021) 1521–1529, https://doi.org/10.1134/S0031918X21140039.
[8] F. Bartolomeu, M. Buciumeanu, E. Pinto, N. Alves, O. Carvalho, F.S. Silva, G. Miranda, 316L stainless steel mechanical and tribological behavior—A comparison between selective laser melting, hot pressing and conventional casting, Addit Manuf 16 (2017) 81–89, https://doi.org/10.1016/j.addma.2017.05.007.
[9] P. Dirisu, S. Ganguly, A. Mehmanparast, F. Martina, S. Williams, Analysis of fracture toughness properties of wire + arc additive manufactured high strength low alloy structural steel components, Mater. Sci. Eng. A 765 (2019), https://doi.org/10.1016/j.msea.2019.138285.
[10] G.G. Goviazin, A. Shirizly, D. Rittel, Static and dynamic mechanical properties of wire and arc additively manufactured SS316L and ER70S6, Mech. Mater. 164 (2022), https://doi.org/10.1016/j.mechmat.2021.104108.
[11] C. Huang, P. Kyvelou, L. Gardner, Stress-strain curves for wire arc additively manufactured steels, Eng Struct 279 (2023), https://doi.org/10.1016/j.engstruct.2023.115628.
[12] M. Sanjari, M. Mahmoudiniya, H. Pirgazi, S. Tamimi, M.H. Ghoncheh, A. Shahriairi, A. Hadadzadeh, B.S. Amirkhiz, M. Purdy, E.G. de Araujo, L. Kestens, M. Mohammadi, Microstructure, texture, and anisotropic mechanical behavior of selective laser melted maraging stainless steels, Mater Charact 192 (2022), https://doi.org/10.1016/j.matchar.2022.112185.

[13] U. Tripathi, N. Saini, R.S. Mulik, M.M. Mahapatra, Effect of build direction on the microstructure evolution and their mechanical properties using GTAW based wire arc additive manufacturing, CIRP J Manuf Sci Technol 37 (2022) 103–109, https://doi.org/10.1016/j.cirpj.2022.01.010.

[14] W. Zhai, N. Wu, W. Zhou, Effect of Interpass Temperature on Wire Arc Additive Manufacturing Using High-Strength Metal-Cored Wire, Metals (basel) 12 (2022), https://doi.org/10.3390/met12020212.

[15] S.I. Evans, J. Wang, J. Qin, Y. He, P. Shepherd, J. Ding, A review of WAAM for steel construction – Manufacturing, material and geometric properties, design, and future directions, Structures 44 (2022) 1506–1522, https://doi.org/10.1016/j.istruc.2022.08.084.

[16] T. Ron, G.K. Levy, O. Dolev, A. Leon, A. Shirizly, E. Aghion, Environmental behavior of low carbon steel produced by a wire arc additive manufacturing process, Metals (basel) 9 (2019), https://doi.org/10.3390/met9080888.

[17] T. DebRoy, H.L. Wei, J.S. Zuback, T. Mukherjee, J.W. Elmer, J.O. Milewski, A.M. Beese, A. Wilson-Heid, A. De, W. Zhang, Additive manufacturing of metallic components – Process, structure and properties, Prog Mater Sci 92 (2018) 112–224, https://doi.org/10.1016/j.pmatsci.2017.10.001.

[18] X. Guo, P. Kyvelou, J. Ye, L.H. Teh, L. Gardner, Experimental study of DED-arc additively manufactured steel double-lap shear bolted connections, Eng Struct 281 (2023), https://doi.org/10.1016/j.engstruct.2023.115736.

[19] Y. Liu, J. Ye, Y. Yang, G. Quan, Z. Wang, W. Zhao, Y. Zhao, Experimental study on wire and arc additively manufactured steel double-shear bolted connections, Journal of Building Engineering 76 (2023), https://doi.org/10.1016/j.jobe.2023.107330.

[20] W. Zuo, M.T. Chen, S.W. Liu, X. Yun, O. Zhao, Y. Huang, B. Cheng, Experimental investigation on double-lap shear behavior of 3D printed austenitic stainless steel bolted connections, Eng Struct 317 (2024), https://doi.org/10.1016/j.engstruct.2024.118501.

[21] Y. Liu, J. Ye, J. He, H. Lu, G. Quan, Z. Wang, Y. Zhao, Testing and design of wire and arc additively manufactured steel double-shear bolted connections with thick plates, J Constr Steel Res 224 (2025), https://doi.org/10.1016/j.jcsr.2024.109069.

[22] X. Guo, P. Kyvelou, J. Ye, L.H. Teh, L. Gardner, Experimental investigation of wire arc additively manufactured steel single-lap shear bolted connections, Thin-Walled Struct. 181 (2022), https://doi.org/10.1016/j.tws.2022.110029.

[23] W. Zuo, M.T. Chen, O. Zhao, A. Su, S.W. Liu, F. Xu, Y. Huang, B. Cheng, Behavior of wire arc additively manufactured 316L austenitic stainless steel single shear bolted connections, Thin-Walled Struct. 202 (2024), https://doi.org/10.1016/j.tws.2024.112075.

[24] W. Zuo, M.T. Chen, O. Zhao, A. Su, S.W. Liu, X. Yun, F. Xu, Structural performance of wire arc additively manufactured duplex stainless steel single-lap shear bolted connections, Eng Struct 319 (2024), https://doi.org/10.1016/j.engstruct.2024.118706.

[25] BS EN 1993-1-8, Eurocode 3. Design of steel structures. Part 1-8: joints, British Standards Institute (2024).

[26] ANSI/AISC 370, Specification for Structural Stainless Steel Buildings, (2021).

[27] Astm e8, e8m,, Standard Test Methods for Tension Testing of Metallic Materials, International and American Society for Testing Materials. (2024).

[28] V. Laghi, M. Palermo, L. Tonelli, G. Gasparini, L. Ceschini, T. Trombetti, Tensile properties and microstructural features of 304L austenitic stainless steel produced by wire-and-arc additive manufacturing, Int. J. Adv. Manuf. Technol. 106 (2020) 3693–3705, https://doi.org/10.1007/s00170-019-04868-8.

[29] IS0 273, Fasteners - Clearance holes for bolts and screws, International Organization for Standardization 1979.